

## The Pacific Ocean

After these two lengthy excursions into polar oceanography we are now ready to test our understanding of ocean dynamics by looking at one of the three major ocean basins. The Pacific Ocean is not everyone's first choice for such an undertaking, mainly because the traditional industrialized nations border the Atlantic Ocean; and as science always follows economics and politics (Tomczak, 1980), the Atlantic Ocean has been investigated in far more detail than any other. However, if we want to take the summary of ocean dynamics and water mass structure developed in our first five chapters as a starting point, the Pacific Ocean is a much more logical candidate, since it comes closest to our hypothetical ocean which formed the basis of Figures 3.1 and 5.5. We therefore accept the lack of observational knowledge, particularly in the South Pacific Ocean, and see how our ideas of ocean dynamics can help us in interpreting what we know.

### Bottom topography

The Pacific Ocean is the largest of all oceans. In the tropics it spans a zonal distance of 20,000 km from Malacca Strait to Panama. Its meridional extent between Bering Strait and Antarctica is over 15,000 km. With all its adjacent seas it covers an area of  $178 \cdot 10^6 \text{ km}^2$  and represents 40% of the surface area of the world ocean, equivalent to the area of all continents. Without its Southern Ocean part the Pacific Ocean still covers  $147 \cdot 10^6 \text{ km}^2$ , about twice the area of the Indian Ocean.

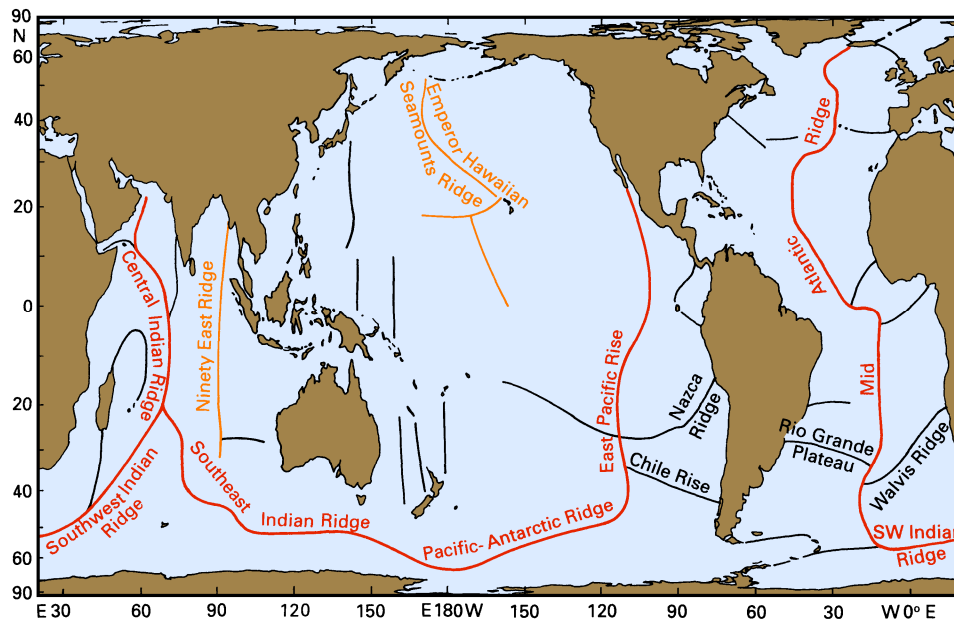


Fig. 8.1. The inter-oceanic ridge system of the world ocean (heavy line) and major secondary ridges. Structures with significant impact on ocean currents and properties are labelled.



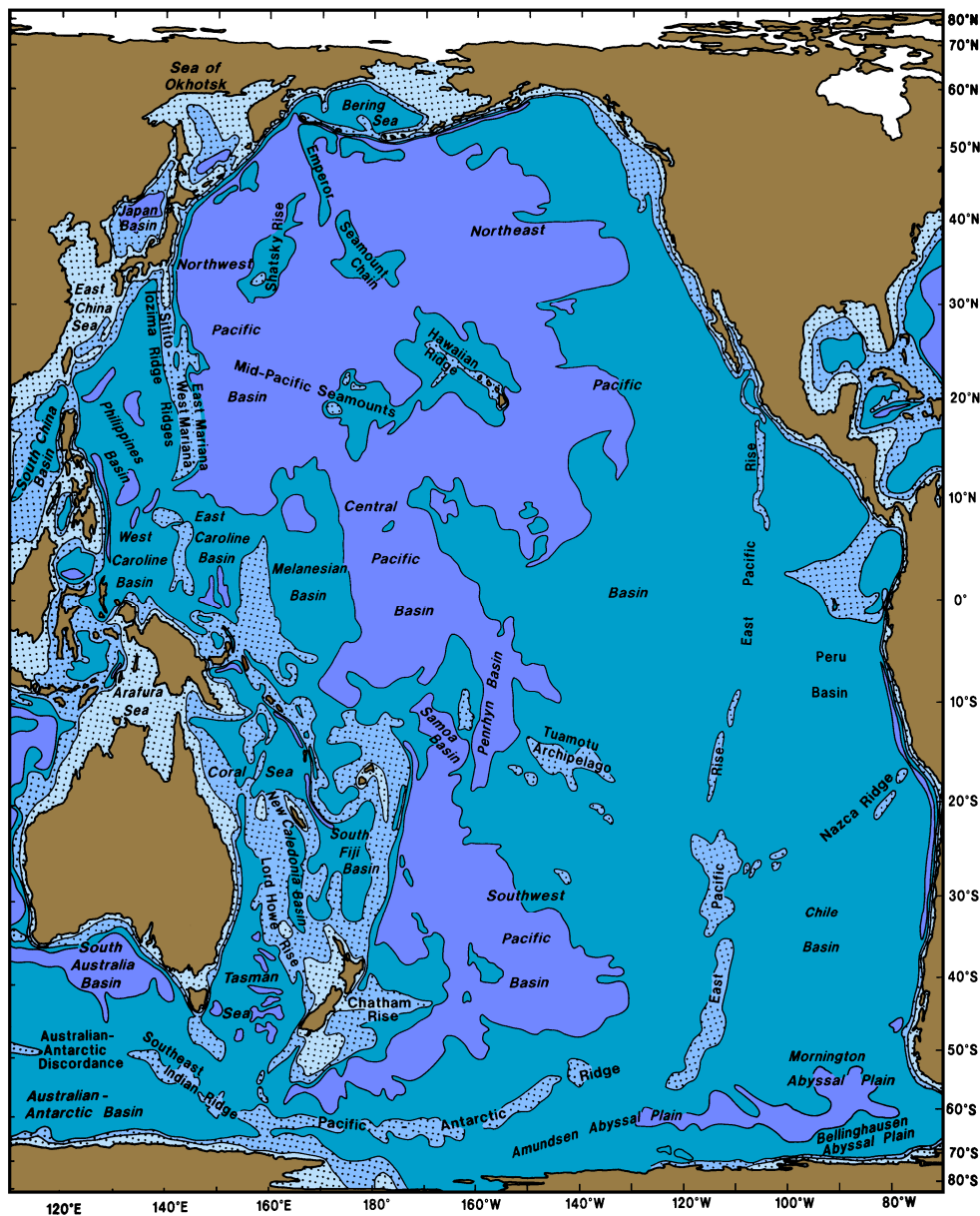


Fig. 8.3. Topography of the Pacific Ocean. The 1000, 3000, and 5000 m isobaths are shown, and regions less than 3000 m deep are shaded.

The inter-oceanic ridge system divides the Atlantic and Indian Oceans into compartments of roughly equal size. In the Pacific Ocean it runs close to the eastern boundary, producing divisions of the southeastern Pacific Ocean similar in size to the Atlantic and Indian basins. The vast expanse of deep ocean in the central and northern Pacific Ocean, on the other hand,



### The wind regime

The atmospheric circulation over the Pacific Ocean is shown in Figures 1.2 - 1.4. The northern Trades are the dominant feature in the annual mean. They are comparable in strength to the Trades in the Atlantic and southern Indian Ocean and make it difficult to see why the ocean received its reputation as the "pacific", or peaceful, ocean. The justification for the name is found in the southern hemisphere where east of 170°W the Trades are moderate or weak but extremely steady. Seasonal variations are also smaller south of the equator, since the belt of high pressure located at 28°S during winter is maintained during summer (January), pushed southward to 35°S by the heat low over the Australian continent, Papua New Guinea, and the Coral Sea. East of 170°W the distribution of air pressure changes little, and the Trades and Westerlies display correspondingly little seasonality there. The effect of the Australian summer low is felt west of 170°W; in the northern Coral Sea across to Vanuatu it produces a monsoonal wind pattern: during winter (June - September) the Trades provide southeasterly air flow, during summer (December - March) the North-west Monsoon blows from Papua New Guinea and Cape York.

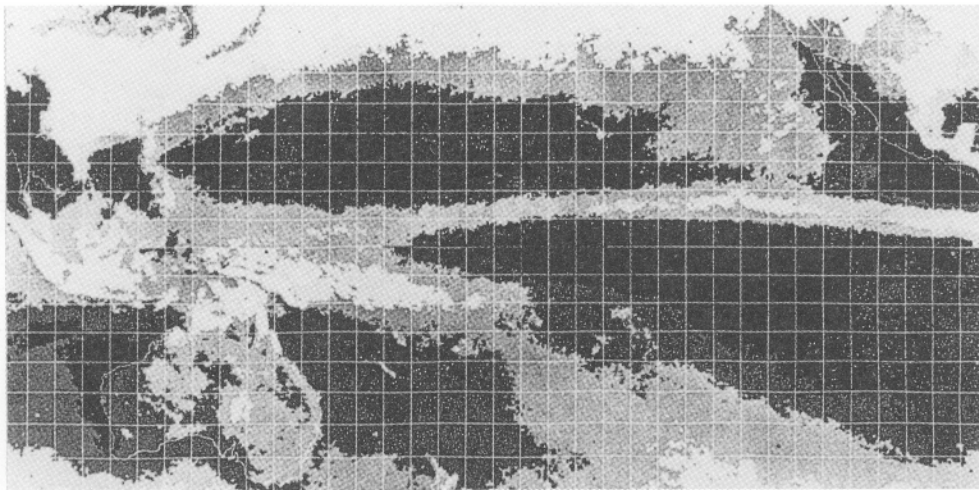


Fig. 8.5. The Intertropical Convergence Zone (ITCZ) and the South Pacific Convergence Zone (SPCZ) as seen in satellite cloud images. The figure is a composite of many months of observations, which makes the cloud bands come out more clearly. It covers the region 40°S - 40°N, 97°E - 87°W; the grid gives every 5° latitude and longitude.

The Trades and the Westerlies of both hemispheres are stronger in winter (July in the south, January in the north) than in summer. North of 55°N this is also true for the polar Easterlies which are barely noticeable in July but very strong in January when the Aleutian low and the Asian high are fully developed; the cyclonic winter circulation associated with the Aleutian low is so strong that it determines the annual mean. The Asian winter high extends a fair way over the ocean and produces a wind reversal over the East and South



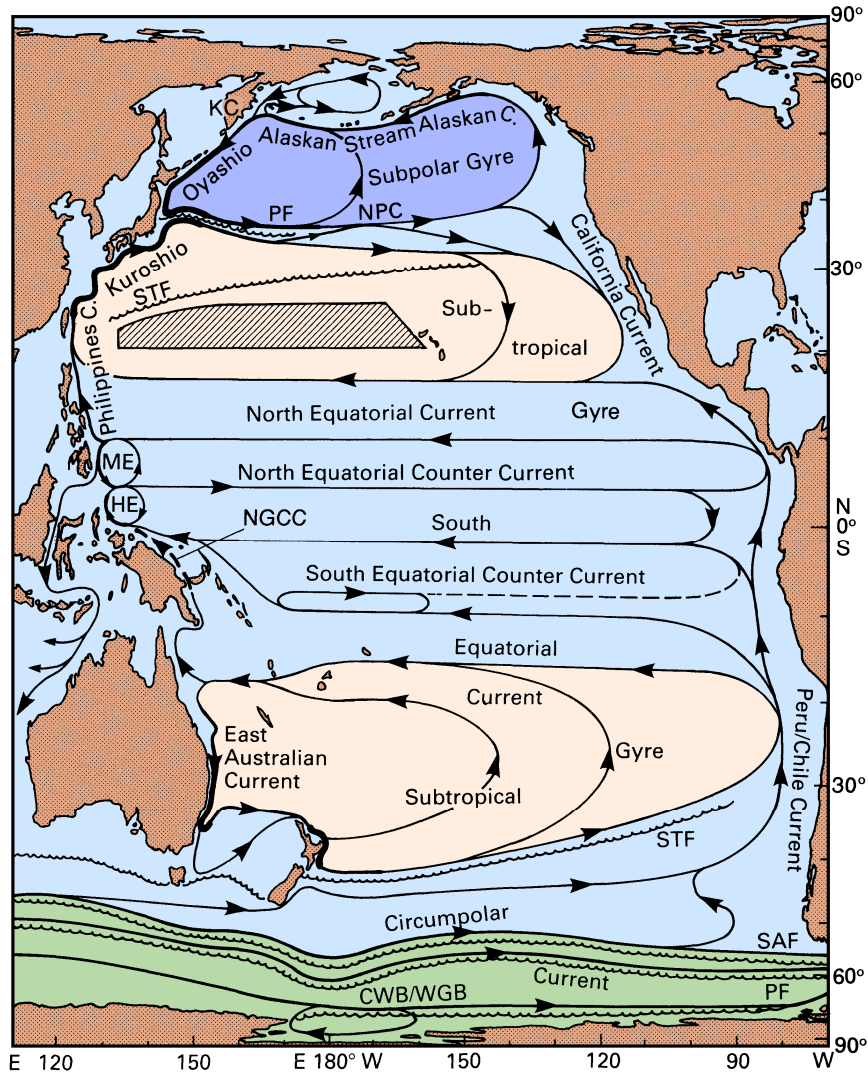


Fig. 8.6. Surface currents of the Pacific Ocean. Abbreviations are used for the Mindanao Eddy (ME), the Halmahera Eddy (HE), the New Guinea Coastal (NGCC), the North Pacific (NPC), and the Kamchatka Current (KC). Other abbreviations refer to fronts: NPC: North Pacific Current, STF: Subtropical Front, SAF: Subantarctic Front, PF: Polar Front, CWB/WGB: Continental Water Boundary / Weddell Gyre Boundary. The shaded region indicates banded structure (Subtropical Countercurrents). In the western South Pacific Ocean the currents are shown for April - November when the dominant winds are the Trades. During December - March the region is under the influence of the northwest monsoon, flow along the Australian coast north of 18°S and along New Guinea reverses, the Halmahera Eddy changes its sense of rotation and the South Equatorial Current joins the North Equatorial Countercurrent east of the eddy. Flow along the STF is now called the South Pacific Current (Stramma *et al.*, in press).



200 m depth in the west, rises to 40 m or less in the east and shows typical speeds of up to  $1.5 \text{ m s}^{-1}$ . Surface flow above the EUC is usually to the west, and the EUC does not appear in reports of ship drift. Although it is the swiftest of all equatorial currents its existence remained unknown to oceanographers until 1952 when it was discovered by Townsend Cromwell and Ray Montgomery. None of the theories of ocean dynamics at the time predicted eastward subsurface flow at the equator. The discovery of the Atlantic Equatorial Undercurrent by Buchanan 80 years earlier (see Chapter 14) had been forgotten, and the discovery of the Pacific EUC was therefore a major event in oceanography; for a few years after Cromwell's death the Undercurrent was called the Cromwell Current.

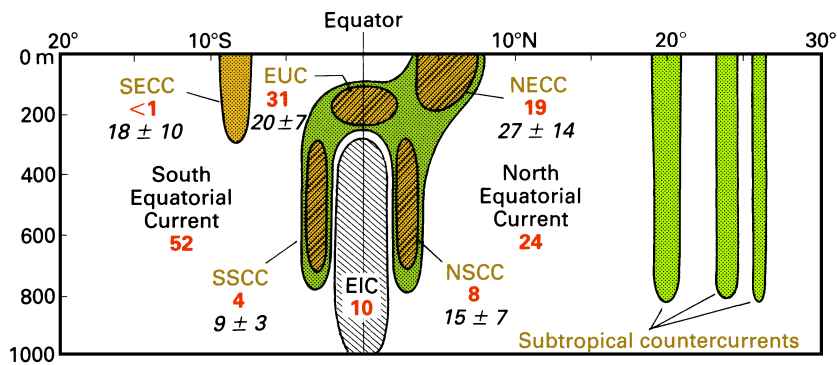


Fig. 8.7. A sketch of the structure of the equatorial current system in the central Pacific Ocean ( $170^\circ\text{W}$ ). Eastward flow is coloured. All westward flow north of  $5^\circ\text{N}$  constitutes the North Equatorial Current, westward flow south of  $5^\circ\text{N}$  outside the EIC represents the South Equatorial Current. EUC = Equatorial Undercurrent, EIC = Equatorial Intermediate Current, NECC and SECC = North and South Equatorial Countercurrents, NSCC and SSCC = North and South Subsurface Countercurrents. Transports in Sverdrups are given for  $155^\circ\text{W}$  (bold figures; based on observations from April 1979 - March 1980) and  $165^\circ\text{E}$  (italics, based on January 1984 - June 1986).

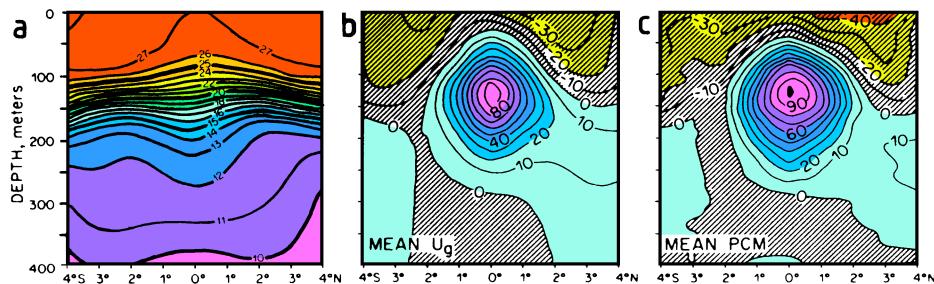


Fig. 8.8. The Equatorial Undercurrent during February 1979 - June 1980 near  $155^\circ\text{W}$ . (a) Mean temperature ( $^\circ\text{C}$ ), (b) mean geostrophic zonal velocity ( $10^{-2} \text{ m s}^{-1}$ ), (c) mean observed zonal velocity ( $10^{-2} \text{ m s}^{-1}$ ). Note the spreading of the isotherms at the equator. From Lukas and Firing (1984).



Countercurrent. Evidence for strong separation is found in the T-S characteristics. Figure 8.10 shows T-S curves from the region north of Papua New Guinea. The change from high salinity water of southern origin to low salinity northern water occurs within 250 km between 1°S and 2°N. That this separation of the circulation is maintained towards the east is seen in the distribution of tritium introduced into the ocean from atmospheric bomb tests during the late 1950s and early 1960s. These tests were all performed in the northern hemisphere; tritium entered the thermocline through subduction at the northern Subtropical Convergence and quickly reached the equatorial current system. In 1973 - 1974 tritium levels surpassed 4 TU (1 TU = 1 tritium atom per  $10^{18}$  hydrogen atoms) north of 3°N and had reached 9 TU near 12°N. In comparison, tritium values south of 3°N were close to 1.5 TU (Fine *et al.*, 1987).

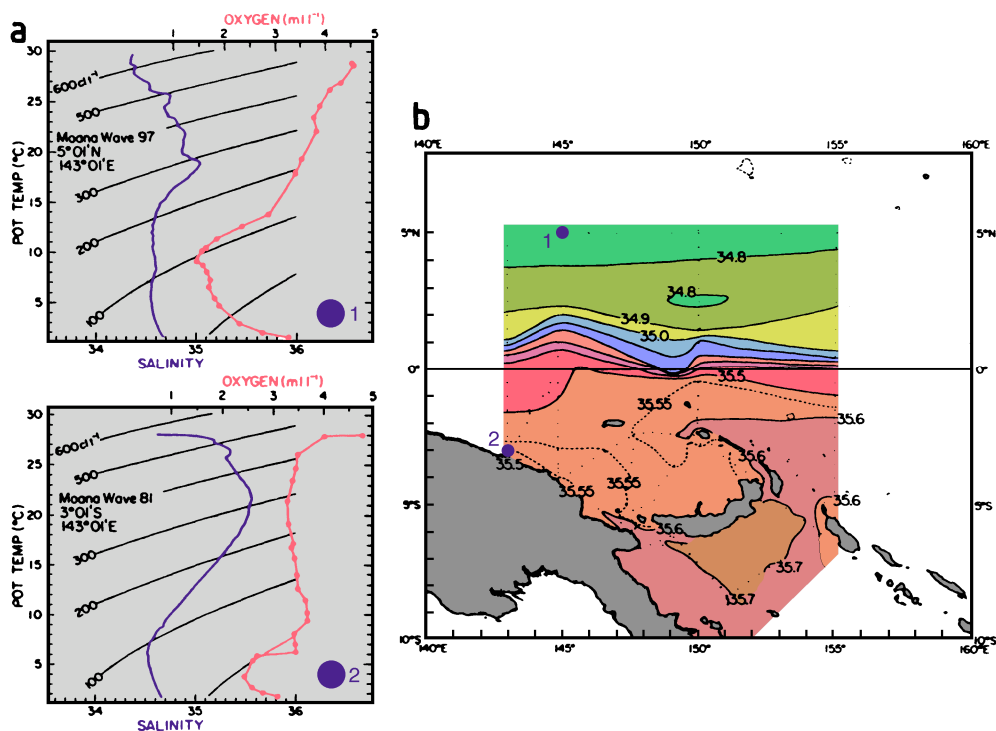


Fig. 8.10. Evidence for separation between northern and southern hemisphere circulation systems in the Pacific thermocline. (a) T-S diagrams and T-O<sub>2</sub> diagrams (identified by circles) from two stations north of Papua New Guinea, (b) salinity on an isopycnal surface located at approximately 180 m depth. Note the difference in maximum salinity and the crowding of the isohalines between the equator and 3°N. From Tsuchiya *et al.* (1989).

From the location of the separation zone north of the equator it can be concluded that the Equatorial Undercurrent belongs entirely to the southern circulation system. Observations show that its source waters originate nearly exclusively from the southern hemisphere. Most of the 8 Sv transported by the EUC past 143°E can be traced back to the South



Significant loss of water from the current is indicated by the strong eastward decrease of its transport. Historical data indicate that in the eastern Pacific Ocean most of this loss occurs to the south.

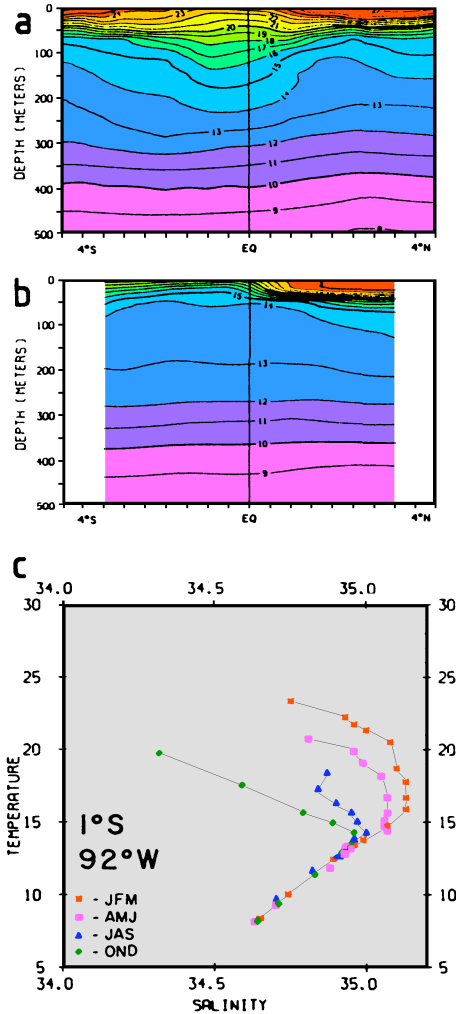


Fig. 8.12 (left). Seasonal variability of the Equatorial Undercurrent in the termination region at 92°W.

(a) Mean temperature (°C) for January - March,

(b) mean temperature (°C) for October - December,

(c) seasonal mean T-S curves. Low salinity and the absence of isotherm spreading in October - December indicate the absence of the Undercurrent. From Lukas (1986).

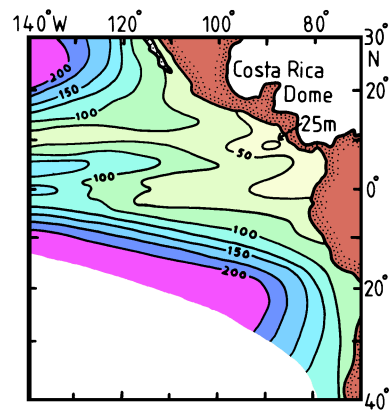


Fig. 8.13. Annual mean depth of the thermocline in the eastern Pacific Ocean, showing the Costa Rica Dome. After Voituriez (1981).

The major westward components of the equatorial current system are the *North Equatorial Current* (NEC) and the *South Equatorial Current* (SEC). Both are directly wind-driven and respond quickly to variations in the wind field. They are therefore strongly seasonal and reach their greatest strength during the winter of their respective hemispheres when the Trades are strongest. The NEC carries about 45 Sv with speeds of 0.3 m s<sup>-1</sup> or less; it is strongest in February. The SEC is strongest in August when it reaches speeds of 0.6 m s<sup>-1</sup>. Its transport at the longitude of Hawaii (155°W) is then about 27 Sv; this



On approaching Australia the South Equatorial Current bifurcates near 18°S; part of it feeds the East Australian Current, while its northern part continues northward along the Great Barrier Reef and through the Solomon Sea and passes through Vitiaz Strait to feed the North Equatorial Countercurrent and the Equatorial Undercurrent. This northern path is suppressed near the surface during the Northwest Monsoon season (December - March) but continues below the then prevailing southward surface flow as the Great Barrier Reef Undercurrent (Figure 8.11). The SEC therefore continues to feed the Equatorial Undercurrent during the monsoon season but does not supply source waters for the North Equatorial Countercurrent during those months.

The *Equatorial Intermediate Current* (EIC) is an intensification of westward flow within the general westward movement of the SEC. Observations over 30 months at 165°E gave an average westward transport of  $7.0 \pm 4.8$  Sv with speeds above  $0.2 \text{ m s}^{-1}$  near 300 m. At 150 - 160°W its core is consistently found with speeds above  $0.1 \text{ m s}^{-1}$  near 900 m. At the same latitudes the cores of the *South Subsurface Countercurrent* and the *North Subsurface Countercurrent* are usually located near 600 m. An explanation for the existence of these currents is still lacking. Recent observations indicate that the banded structure of currents at the equator continues to great depth (Figure 8.15). Below the permanent thermocline currents exceeding  $0.2 \text{ m s}^{-1}$  are quite rare in the open ocean, and the existence of such currents near the equator indicates that the dynamics of the equatorial region cannot be explained by our  $1\frac{1}{2}$  layer model. The EIC, NSCC, and SSCC are integral parts of a dynamic system that reaches much deeper than the thermocline. The fact that the Costa Rica Dome is a permanent feature despite strong seasonality of the North Equatorial Countercurrent indicates that the NSCC also plays a part in maintaining the thermocline structure in the Dome.

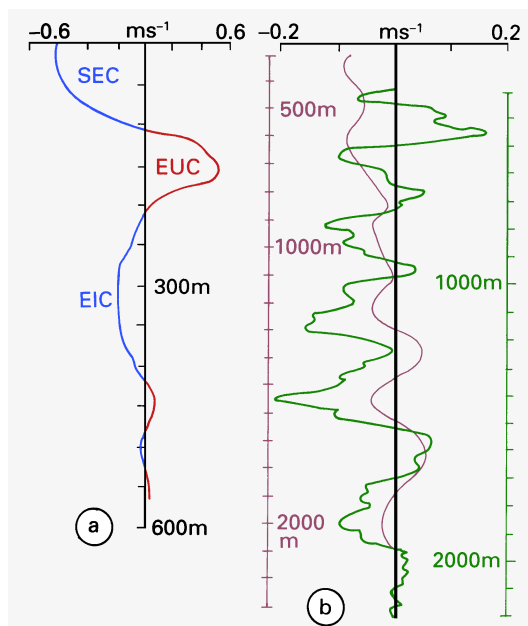


Fig. 8.15. Evidence for banded structure of currents at the equator.

(a) The South Equatorial Current (SEC), Equatorial Undercurrent (EUC), and Equatorial Intermediate Current (EIC) at 165°E;

(b) deep equatorial currents at 150 - 160°W during 1980 (solid line, right depth scale) and during March 1982 - June 1983 (thin line, left depth scale). The cores of all current bands coincide if the entire current system during 1982/83 is shifted upward some 130 m.

Note the different depth and velocity scales. Adapted from Delcroix and Henin (1988) and Firing (1987).



Evidence for a South Subtropical Countercurrent in the Coral Sea was presented by Donguy and Henin (1975).

### Western boundary currents

We begin the discussion of western boundary currents with the *Kuroshio* or "black (i.e. unproductive) current". All western boundary currents have a number of features in common: They flow as swift narrow streams along the western continental rise of ocean basins; they extend to great depth well below the thermocline; and they separate at some point and continue into the open ocean as narrow jets, developing instabilities along their paths. These features result from general hydrodynamic principles and reflect the balance of forces in the western boundary regions of the subtropical and subpolar gyres (the closure of the Sverdrup regime). Additional characteristics are imposed by the topography and give each boundary current its own individuality. The characteristic feature of the *Kuroshio* is that it has several quasi-stable paths. A complete description of the *Kuroshio* system therefore includes a number of alternative pathways (Figure 8.16). The current begins where the North Equatorial Current approaches the Philippines and continues northward east of Taiwan. It crosses the ridge that connects Taiwan with the Okinawa Islands and Kyushu and continues along the continental rise east of the East China Sea. As the ridge is less than 1000 m deep the current is relatively shallow in this region. It responds to the ridge crossing by forming the East China Sea meander. The meander shows some seasonality in strength and position, increasing in amplitude and moving northeastward in winter. Oscillations with periods of 10 - 20 days and wavelengths of 300 - 350 km occur along the *Kuroshio* front but the path along the East China Sea is quite stable otherwise. The Tsushima Current branches off from the *Kuroshio* near 30°N (see Chapter 10).

South of Kyushu the *Kuroshio* passes through Tokara Strait, a passage also not deeper than 1000 m, and bends sharply to the left. Downstream from Tokara Strait it has been observed near the 1000 - 1500 m isobaths to be only 600 m deep, with velocities above  $1.0 \text{ m s}^{-1}$  at the surface,  $0.5 \text{ m s}^{-1}$  near 400 m, and southwestward flow (i.e. opposed to the surface movement) of up to  $0.2 \text{ m s}^{-1}$  below. Geostrophic calculations indicate that even in 4000 m of water the current does not reach much beyond 1500 m depth. Further downstream along the continental rise of Japan the Izu Ridge south of Honshu forms another obstacle to the flow. The current negotiates it along one of three paths. In the "large meander" path the current turns southeastward near 135°E and flows northward along the ridge before crossing it close to the coast (path 3 in Figure 8.16). In the "no large meander" path it alternates between a path that follows the coast closely (path 1) and a small meander across the ridge (path 2). As shown in Figure 8.16 the change from paths 1 or 2 to the large meander situation occurs every few years at irregular intervals. During those years when the *Kuroshio* does not follow the large meander path the current changes between paths 1 and 2 about every 18 months. What causes the *Kuroshio* to change its path remains to be fully explained. Observations show a distinct increase in velocity before the current changes from the large meander path to paths 1 or 2. This suggests some kind of hydraulic control exerted by the Izu Ridge.



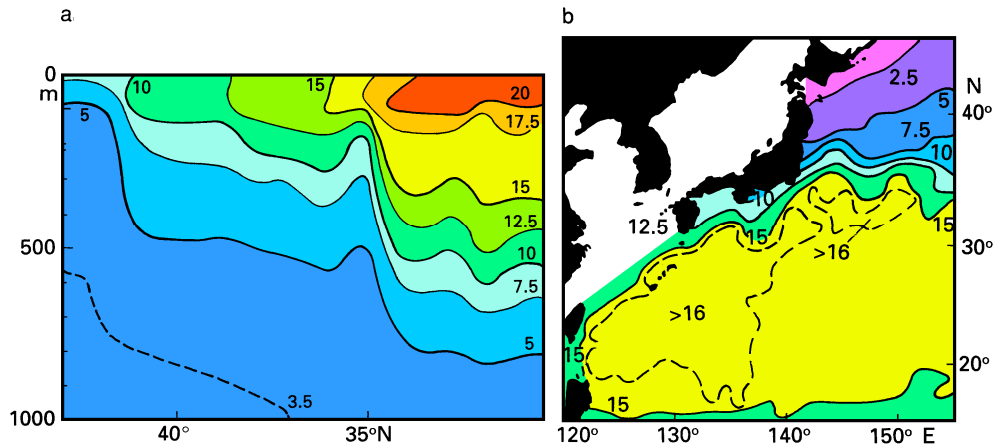


Fig. 8.17. The Kuroshio in the oceanic temperature field. (a) Vertical section of temperature (°C) across the Kuroshio Extension along 165°E, (b) temperature (°C) at 300 m depth. From Joyce (1987) and Stommel and Yoshida (1972).

Downstream from its separation point the Kuroshio continues into open water as a free inertial jet. Such jets create instabilities along their paths which develop into eddies or rings. In a map of eddy energy in the world ocean (Figure 4.8) the Kuroshio Extension therefore stands out as one of the regions with very high eddy energy. The process of ring formation is described in detail in Chapter 14 for the Gulf Stream, where more observations of the phenomenon are available. Kuroshio rings behave very much the same, so what is said in that chapter is relevant here as well. Observations over many years indicate that the Kuroshio forms about 5 rings every year when it flows along one of its stable paths and about 10 rings during years of transition. Kuroshio rings extend to great depth; analysis of long-term current meter measurements indicates coherence of kinetic energy virtually to the ocean floor. Eddy kinetic energy falls off across the Emperor Seamounts to one fifth of the amount observed in the west. Observations of deep flow over a one-year period (Schmitz, 1987) revealed unusually strong abyssal currents of  $0.05 - 0.06 \text{ m s}^{-1}$  below 4000 m depth just west of the Emperor Seamounts. These currents were directed westward near 165°E at either side of the Kuroshio Extension but eastward through a gap between two seamounts at 171°E, under the axis of the surface jet. The flow direction and strength was extremely stable and not reversed by eddies. In contrast, abyssal flow east of the Emperor Seamounts is so weak that it is regularly reversed by eddies, despite their lower energy levels there.

As in other western boundary currents, transport in the Kuroshio increases along its path, indicating entrainment of water from the subtropical gyre. In the Kuroshio Extension near 152°E and 165°E it has been estimated at 57 Sv, which is close to the 50 Sv estimated from closing the integrated Sverdrup flow. The current flows strongest during summer; seasonal variation of the sea level difference across Tokara Strait (0.6 m in the annual mean) indicates an increase of 13% from winter to summer. This apparently contradicts the



The southward boundary of the Oyashio with temperatures of 2 - 8°C defines the Polar Front; it is usually located at 39 - 40°N. Occasionally (for example during 1963, 1981, and 1984) the Oyashio pushes south as far as 36°N. This appears to occur when the region of zero wind stress curl moves southward, apparently extending the subpolar gyre southward by some 300 - 500 km. The southern edge of the Oyashio and the northern edge of the Kuroshio maintain their own frontal systems along the Kuroshio Extension. Thus, in the section shown in Figure 8.17a which is located about half-way between the Shatsky Rise and the Emperor Seamounts, the Kuroshio Front is seen at 35°N (identified by the 15°C isotherm) and the Oyashio or Polar Front at 41°N (the 5°C isotherm). The two fronts are associated with geostrophic flow, the front at 35°N with the 57 Sv of the Kuroshio and the front at 41°N with another 22 Sv as the continuation of the Oyashio. Between the two flows and on either side movement is weakly westward.

The Oyashio is the continuation of two currents. The *Kamchatka Current* brings water from the Bering Sea southward. It is associated with quasi-permanent anticyclonic eddies on the inshore side which are caused by bottom topography and coastline configuration and result in countercurrents along the coast. The larger of the two Oyashio sources is the *Alaskan Stream*, the extension of the western boundary current along the Aleutian Islands. The distinction between the Alaskan Stream and the Alaska Current further to the east is gradual, and the two currents are sometimes regarded as one. They are, however, of different character, the Alaska Current being shallow and highly variable but the Alaskan Stream reaching to the ocean floor. This indicates that despite its relatively modest speed of 0.2 - 0.3 m s<sup>-1</sup> the latter is a product of western boundary dynamics, while the former belongs to the eastern boundary regime.

No transport estimates are available for the Alaskan Stream over its entire depth. Geostrophic estimates for the transport in the upper kilometer in the region 155 - 175°W vary between 5 and 12 Sv and show a width of the Stream of 150 - 200 km (Royer and Emery, 1987). South of the Stream the *North Pacific Current* continues from the Kuroshio and Oyashio Extension through the region between 30°N and some 200 km off the Alaskan coast, a broad band of eastward flow more than 2000 km wide. Because of the heavy distortion of distances in the subpolar parts of Figure 8.6, the figure cannot adequately portray this difference in width. Some authors distinguish between the North Pacific Current as the continuation of the Kuroshio Extension south of about 43°N and a Pacific Subarctic Current to the north representing the continuation of the Oyashio Front. Whether the clear separation of the Kuroshio and Oyashio Fronts in the west is maintained all across the Pacific basin, effectively suppressing exchange of water between the subtropical and subpolar gyres, is doubtful, and it appears more appropriate to regard all eastward flow south of Alaska part of the same broad current.

A prominent western boundary current of the equatorial current system is the *Mindanao Eddy*. Captains of vessels that carry Australian wealth to Japan know it well and take advantage of it by following the Mindanao coast southward on their way from Japan to western Australia while travelling 100 - 200 km offshore on their way north. Its transport is estimated at between 25 and 35 Sv, with strong interannual variations. Observations in the western part of the eddy (the *Mindanao Current*) show that the equatorward flow does not extend below 250 m; flow in the depth range 250 - 500 m is poleward and carries some 16 - 18 Sv. The *Halmahera Eddy* and the *New Guinea Coastal Current* are seasonal boundary currents near the surface (the latter flows northwestward throughout the year below 200 m, see Fig. 8.11). The flow direction shown in Figure 8.6 reverses during a few



Ocean would be diverted through the Great Australian Bight, doubling the transport of the East Australian Current. The instabilities may result in part from the fact that the current first follows the Australian coast but has to leave it to continue along the eastern coast of New Zealand. The current therefore separates from the Australian coast somewhere near 34°S (the latitude of the northern end of New Zealand's North Island). The path of the current from Australia to New Zealand is known as the Tasman Front, which marks the boundary between the warm water of the Coral Sea and the colder water of the Tasman Sea. This front develops wave-like disturbances (meanders) and associated disturbances in the thermocline which eventually travel westward with Rossby wave speed. When the waves impinge upon the Australian coast they separate from the main current and turn into eddies.

Figure 8.19 shows the process of eddy formation. Because the meander closest to the coast always extends southward and thus can trap water only from the Coral Sea, the East Australian Current spawns many anticyclonic (warm core) but few cyclonic (cold core) eddies. Figure 8.20 shows the current extending to 37°S, flowing back past 34°S before turning eastward and forming the warm eddy "Maria" in the process. A band or "ring" of warm water is clearly seen around the eddy, indicating the region of strongest currents. When the eddy becomes separated from the main current it will maintain its speed ( $1.5 - 2.0 \text{ m s}^{-1}$ ) for many months while its hydrographic structure changes. Eddies that go through winter cooling and subsequent spring warming lose their surface signature and are no longer detectable in satellite observations of sea surface temperature (Figure 8.21). Eddy "Leo" in Figure 8.20 is such an eddy; its presence is revealed by the track of two drifting buoys but not visible in the temperature pattern. Remnants of eddies in the form of subsurface layers of uniform temperature and salinity are abundant south of the Tasman Front and are characteristic of the upper 500 m of the Tasman Sea (Figure 8.22).

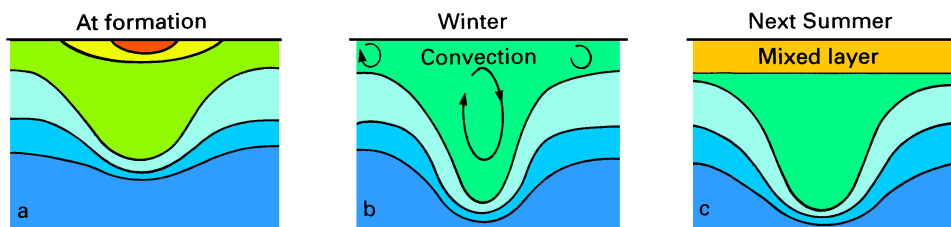


Fig. 8.21. Evolution of the hydrographic structure in an East Australian Current eddy: isotherms in a section across the eddy (a) at the time of formation, (b) during winter, (c) in the following summer. The original warm ring signature at the surface is destroyed by convection from cooling in winter. The eddy is then capped by the seasonal thermocline in the following spring.

The East Australian Current spawns about three eddies per year, and some 4 - 8 eddies may co-exist at any particular time. Because the volume transport in the current is low, the eddies can contain more energy than the current itself. On occasions it is impossible to identify the path of the current; the western boundary current system then is a region of intense eddy activity without well defined mean transport. This is particularly true for the passage of the current from Australia to New Zealand, where an average location of the



Tasman Front can only be defined in statistical terms (Figure 8.23). The current is stronger and reaches further inshore in summer (December - March) than in winter. This is evident from ship drift reports obtained from vessels sailing along the Australian coast between Bass Strait and the Coral Sea. These ships take advantage of the East Australian Current by proceeding along the shelf break on their voyage south; northbound vessels stay inshore of the Current and remain over the shelf. Figure 8.24 shows that during winter northbound vessels occasionally experience an inshore countercurrent to assist their voyage. In summer they may encounter southward flow of more than  $1 \text{ m s}^{-1}$  even on the shelf.

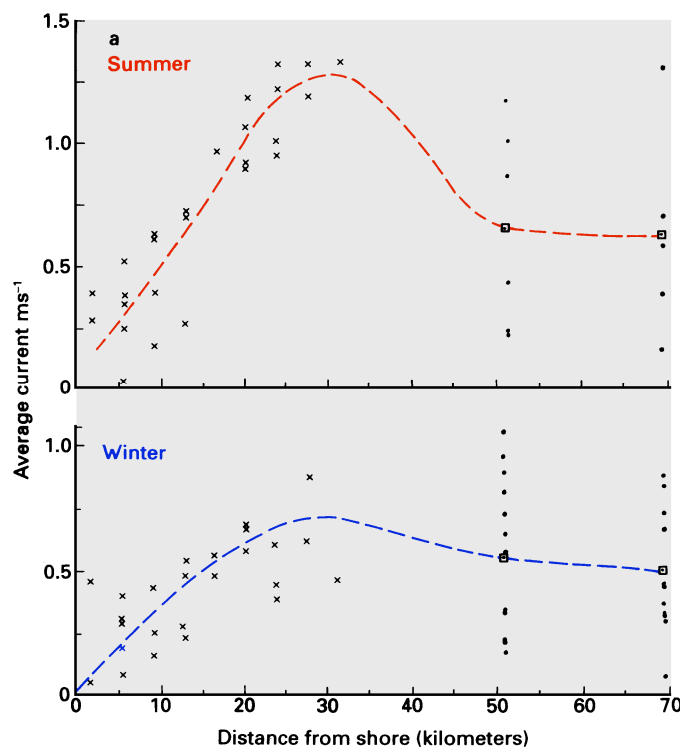


Fig. 8.24. Seasonal variability of the East Australian Current. (a) Mean current velocity for summer and winter near  $30^{\circ}\text{S}$ . See page 130 for part b of the figure. From Godfrey (1973) and Hamon *et al.* (1975).

Fig. 8.23 (page 128). The Tasman Front. Top: Dynamic topography ( $\text{m}^2 \text{s}^{-2}$ ), or steric height multiplied by gravity, as observed in September - October 1979, showing the Tasman Front as a band of large steric height change along the  $18 \text{ m}^2 \text{s}^{-2}$  contour; to obtain approximate steric height in m, divide contour values by 10. Bottom: Mean position of the front as determined from satellite SST observations during March 1982 - April 1985; the front was found during more than 30% of the observation period in the lightly shaded area, more than 50% of the time in the dark region, and always in the black region. Adapted from Stanton (1981) and Mulhearn (1987).



### Eastern boundary currents and coastal upwelling

In the vertically integrated flow, the eastern part of the Pacific Ocean occurs as a region of broad and weak recirculation for the ocean-wide gyres. This is correct for the mean flow away from coastal boundaries but does not hold for currents over short periods and close to the shelf. The aspect of short term variability in the open ocean was already addressed through an example from the Atlantic Ocean (Figure 4.9); the same arguments apply to the Pacific or Indian Oceans. Closer to shore the dynamics are further modified as a result of the meridional direction of the winds. To understand the resulting circulation, known as coastal upwelling, it is necessary to review very briefly the balance of forces along eastern ocean boundaries.

The reason for the strong equatorward component of the Trades along eastern ocean coastlines is the strong difference in climatic conditions between the eastern and western coasts. In the west the Trades impinge on the land laden with moisture which they collected from evaporation over the sea. The coastal regions are therefore well supplied with rainfall; the eastern coastal regions of Madagascar, Brazil, Southeast Asia, New Guinea and the Cape York peninsula of Australia are all covered with luxurious rainforest. At the same latitudes in the east the Trades arrive depleted of moisture, having rained out over the land further east. Lacking the essential rain the coastal regions are deserts: the Simpson desert in Australia, the Atacama desert in South America, the Namib in South Africa, and the Californian desert regions in North America are all found at the same latitudes where rainforests flourish on the opposite side of the oceans. Over these desert lands the air is dry and hot in summer, creating low pressure cells (Figure 1.3). The resulting pressure difference between land and ocean gives rise to equatorward winds along the coast.

The effect of the wind on the oceanic circulation was already demonstrated in Figure 4.1 and is described in more detail in Figure 8.25: The Ekman transport  $E$  produced by equatorward winds is directed offshore; as a result the sea surface is lowered at the coast. The corresponding zonal pressure gradient which develops in a band of about 100 km width along the coast supports a geostrophic flow  $GF$  toward the equator, i.e. in the same direction as the wind. The water that is removed from the coast at the surface has to be supplied from below, hence upward water movement (of a few meters per week) occurs in a narrow region close to the coast. This upwelling water in turn has to be supplied from the offshore region. On a shallow shelf this can occur in a bottom boundary layer as indicated in Figure 8.25b, but outside the shelf flow toward the coast has to be geostrophic. In other words, in addition to the zonal pressure gradient produced by the Ekman transport, a meridional pressure gradient must exist as well, to support the supply of water for the upwelling process. This pressure gradient is directed poleward; geostrophy implies that it is balanced by the Coriolis force linked with the onshore water movement. Close to the coast this movement runs into the shelf and comes to a halt, the associated Coriolis force goes to zero, and we encounter a situation already familiar from the dynamics of the Equatorial Undercurrent: In the absence of an opposing force the pressure field accelerates the water down the pressure gradient, until frictional forces are large enough to prevent further growth of the velocity. The result is poleward flow  $PF$  in a narrow band near and above the shelf break. This flow competes with the equatorward geostrophic flow driven by the zonal pressure gradient. It is therefore usually not observed at the surface but always seen as an undercurrent along the continental slope. Note that similar to western boundary currents or the equatorial undercurrent only the downstream pressure gradient is not in geostrophic



along the eastern boundary. The result is a deflection of isotherms from zonal to meridional orientation along the eastern boundary (Figure 2.5a). The water warms as it moves equatorward and offshore; this is reflected in large net heat fluxes into the ocean (Figure 1.6).

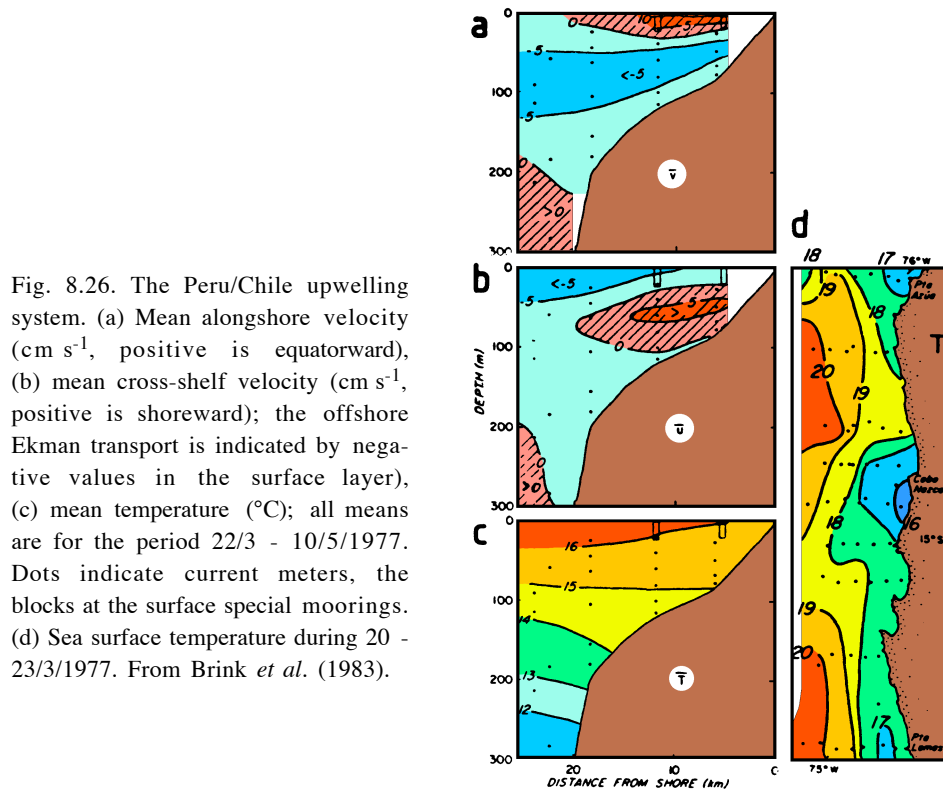


Fig. 8.26. The Peru/Chile upwelling system. (a) Mean alongshore velocity ( $\text{cm s}^{-1}$ , positive is equatorward), (b) mean cross-shelf velocity ( $\text{cm s}^{-1}$ , positive is shoreward); the offshore Ekman transport is indicated by negative values in the surface layer, (c) mean temperature ( $^{\circ}\text{C}$ ); all means are for the period 22/3 - 10/5/1977. Dots indicate current meters, the blocks at the surface special moorings. (d) Sea surface temperature during 20 - 23/3/1977. From Brink *et al.* (1983).

The most impressive coastal upwelling system of the world ocean is found in the *Peru/Chile Current*. This current is strong enough to lower sea surface temperatures along South America by several degrees from the zonal average (Figure 2.5a). Embedded in the current is a vigorous upwelling circulation which lowers the temperatures within 100 km of the coast by another 2 - 4 $^{\circ}\text{C}$ . The coastal upwelling band is too narrow to be resolved by the ocean-wide distribution of Figure 2.5a, so the low temperatures seen on the oceanic scale reflect advection of temperate water in the subtropical gyre. To see the effects of the coastal upwelling circulation we have to take a closer look at the inshore region. Figure 8.26 shows equatorward surface flow above 30 m, the poleward undercurrent between 30 m and 200 m, offshore Ekman transport above 30 m, and onshore movement of water mainly in the range 30 - 100 m with very little onshore or offshore movement below. Onshore transport in coastal upwelling regions does not extend below 400 m at most. The depth range for onshore movement in the Peru/Chile upwelling system is, however, particularly shallow, probably as a result of the extreme narrowness of the shelf.



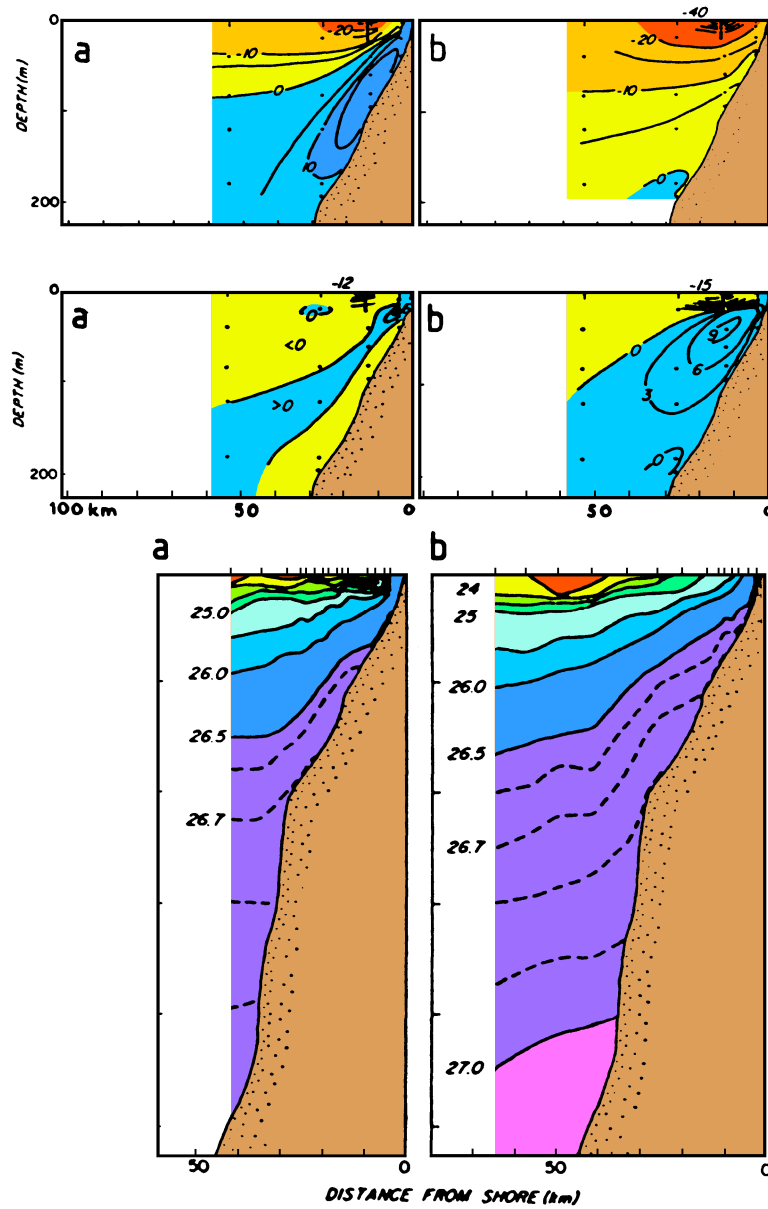


Fig. 8.27. Alongshore flow  $v$  (top;  $\text{cm s}^{-1}$ , positive is poleward), cross-shelf flow  $u$  (middle;  $\text{cm s}^{-1}$ , positive is shoreward), and density  $\sigma_t$  (bottom) in the Californian upwelling system. Left: During weak wind conditions, right: during strong wind conditions. Intensification of upwelling during strong winds is indicated by an increase in  $u$  and an increase in equatorward flow accompanied by a reduced undercurrent. The shallow pycnocline (near  $\sigma_t = 24.5$ ) breaks the surface, forming a front some 20 km offshore during periods of strong upwelling; when the wind relaxes this front recedes towards the coast and may eventually disappear. From Huyer (1976).